# ELASTIC FIELDS AT CORNERS OF HIGHLY STRETCHABLE MATERIALS ARE CONCENTRATED BUT BOUNDED

SAMMY HASSAN,† JASON STECK,† ZHIGANG SUO\*

 $\hbox{JOHN A. PAULSON SCHOOL OF ENGINEERING AND APPLIED SCIENCE, HARVARD UNIVERSITY, CAMBRIDGE, MA 02138, \\ USA$ 

RUBBER CHEMISTRY AND TECHNOLOGY, Vol. 96, No. 4, pp. 478-488 (2023)

#### **ABSTRACT**

Corners concentrate elastic fields and often initiate fracture. For small deformations, it is well established that the elastic field around a corner is power-law singular. For large deformations, we show here that the elastic field around a corner is concentrated but bounded. We conduct computation and an experiment on the lap shear of a highly stretchable material. A rectangular sample was sandwiched between two rigid substrates, and the edges of the stretchable material met the substrates at 90° corners. The substrates were pulled to shear the sample. We computed the large-deformation elastic field by assuming several models of elasticity. The theory of elasticity has no length scale, and lap shear is characterized by a single length, the thickness of the sample. Consequently, the field in the sample was independent of any length once the spatial coordinates were normalized by the thickness. We then lap sheared samples of a polyacrylamide hydrogel of various thicknesses. For all samples, fracture initiated from corners, at a load independent of thickness. These experimental findings agree with the computational prediction that large-deformation elastic fields at corners are concentrated but bounded. [doi:10.5254/rct.2376991]

## INTRODUCTION

Many structures and devices contain corners, which concentrate elastic fields and often initiate fracture. For small deformations, linear elasticity predicts that elastic fields around corners are power-law singular. Analogous to singular elastic fields around crack tips, the singular elastic fields around corners correlate the critical conditions of fracture for various sample geometries and load types. 3,4

Many elastomers and gels are highly stretchable before fracture. For large deformations, the elastic field around a corner in a neo-Hookean material has been recently analyzed.<sup>5,6</sup> The nearcorner elastic field under large deformations obtained by an asymptotic analysis is not power-law singular. This result is in contrast to the singular elastic field predicted by linear elasticity. Steck et al.<sup>6</sup> believed that the large deformation field around the corner obtained by finite element analysis is bounded, but Hui et al.<sup>5</sup> believed it to be logarithmically singular. A soft material with a corner was also previously simulated,<sup>7</sup> but the focus was not to examine the field around the corner, and the mesh used was too coarse to show whether the corner field was singular or not. Incidentally, at crack tips in both linear and nonlinear elastic materials, the energy density is inversely proportional to the distance from the crack tip.<sup>8</sup> Whether the near-corner fields are bounded or logarithmically singular may deserve further investigation. But a logarithmic singularity is weak and may as well be indistinguishable from a bounded field in experiments. How do bounded (or weakly singular) fields affect fracture from corners?

Here we compute the elastic field around a corner using a mesh of a higher resolution, applied strains of larger magnitude, and various material models. These simulations confirm that the elastic field at a corner is concentrated but bounded. We consider lap shear of a highly stretchable material sandwiched between two rigid substrates (Figure 1). The stretchable material is rectangular and meets the substrates at  $90^{\circ}$  corners. The length of the stretchable material L is taken to be much larger

<sup>†</sup>These authors equally contributed to this work.

<sup>\*</sup>Corresponding author. Email: suo@seas.harvard.edu

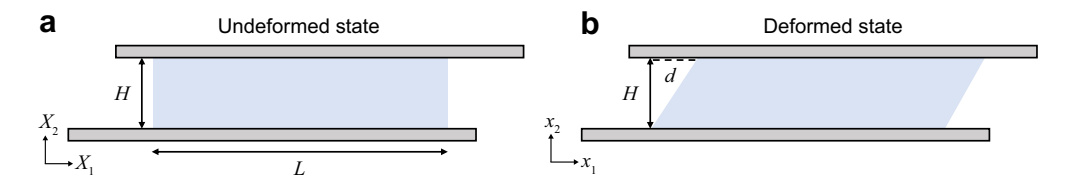


FIG. 1. — Lap shear in the (a) undeformed state and (b) deformed state.

than the thickness H. The width of the stretchable material B is much larger than the thickness, such that, when the substrates are pulled relative to each other by distance d, the stretchable material deforms under the plane strain condition. The magnitude of the bounded field at the corner is amplified from that of the applied field. Experimentally, we lap shear samples of a polyacrylamide hydrogel of various thicknesses. For all samples, fracture initiates from corners, at a critical load independent of thickness. These experimental findings agree with the computational predictions that large-deformation elastic fields at corners are concentrated but bounded.

## VARIOUS MATERIAL MODELS

A neo-Hookean material is specified by the energy density function:

$$W = \frac{\mu}{2} (F_{ik} F_{ik} - 3), \tag{1}$$

where  $F_{ik}$  is the deformation gradient and  $\mu$  is the shear modulus. The material is taken to be incompressible.

A homogeneous shear strain  $\gamma$  corresponds to the deformation gradient:

$$F = \begin{pmatrix} 1 & \gamma & 0 \\ 0 & 1 & 0 \\ 0 & 0 & 1 \end{pmatrix}. \tag{2}$$

Consequently, the energy density is

$$W = \mu \gamma^2 / 2. \tag{3}$$

This result of the neo-Hookean material undergoing large deformation coincides with that of a linear elastic material undergoing infinitesimal deformation.

The components of true stress are given by

$$\sigma_{ii} = \mu F_{ik} F_{ik} - \rho \delta_{ii}, \tag{4}$$

where  $\rho$  is the Lagrange multiplier that enforces incompressibility and corresponds to a hydrostatic pressure. A direct calculation gives

$$\sigma = \begin{pmatrix} \mu(1+\gamma^2) - \rho & \mu\gamma & 0\\ \mu\gamma & \mu - \rho & 0\\ 0 & 0 & \mu - \rho \end{pmatrix}. \tag{5}$$

In simple shear, the hydrostatic pressure is undetermined, and all normal stress components are nonzero. The differences in normal stresses are given by  $\sigma_{11} - \sigma_{22} = \sigma_{11} - \sigma_{33} = \mu \gamma^2$ . The shear stress components are given by  $\sigma_{12} = \sigma_{21} = \mu \gamma$ . The nonzero normal stresses are called the Poynting effect.<sup>9</sup>

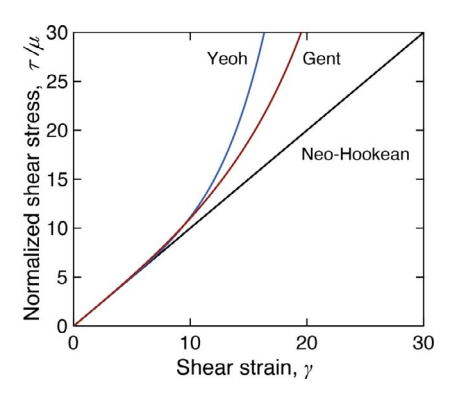


FIG. 2. — Stress–strain curves of several models of elasticity under simple shear. For the Yeoh model, we take  $C_2/C_1 = -4 \times 10^{-5}$  and  $C_3/C_1 = 4 \times 10^{-6}$ . For the Gent model, we set  $J_m = 1089$ .

A Mooney–Rivlin material model<sup>10</sup> is specified by the energy density:

$$W = C_1(I_1 - 3) + C_2(I_2 - 3), (6)$$

where  $C_1$  and  $C_2$  are material constants and  $I_1$  and  $I_2$  are related to the three principal stretches as

$$I_1 = \lambda_1^2 + \lambda_2^2 + \lambda_3^2, \ I_2 = \lambda_1^2 \lambda_2^2 + \lambda_1^2 \lambda_3^2 + \lambda_2^2 \lambda_3^2.$$
 (7)

In plane strain,  $\lambda_3 = 1$ , and for an incompressible material,  $\lambda_1 \lambda_2 \lambda_3 = 1$ . Under these conditions,  $I_1 = I_2 = \lambda_{12} + \lambda_{22} + 1$ . The Mooney–Rivlin material model becomes

$$W = (C_1 + C_2)(I_1 - 3). (8)$$

This expression is identical to that of an incompressible neo-Hookean material, in which the shear modulus is related to the Mooney–Rivlin constants as  $\mu = 2(C_1 + C_2)$ .

A Yeoh material<sup>11</sup> is specified by the energy density:

$$W = C_1(I_1 - 3) + C_2(I_1 - 3)^2 + C_3(I_1 - 3)^3.$$
(9)

The shear modulus is given by  $\mu=2C_1$ , and  $C_2$  and  $C_3$  and are material constants. Under simple shear  $I_1=\gamma^2+3$ , such that  $W=\mu\gamma^2/2+C_2\gamma^4+C_3\gamma^6$ . For small strains, the higher-order terms can be neglected, and the Yeoh model reduces to neo-Hookean.

A Gent material<sup>12</sup> is specified by the energy density:

$$W = -\frac{\mu J_m}{2} \ln \left( 1 - \frac{I_1 - 3}{J_m} \right),\tag{10}$$

where  $\mu$  is the shear modulus at small strain and  $J_m$  is a fitting parameter. Under simple shear,  $W = -\mu/2 J_m \ln(1 - \gamma^2/J_m)$ . When  $J_m \to \infty$ , the Gent model reduces to neo-Hookean.

The stress–strain curves for the various material models agree at small strain but disagree at large strain (Figure 2). As noted above, a Mooney–Rivlin material is indistinguishable from a neo-Hookean material in plane strain. We will not consider the Mooney–Rivlin material further in this article.

## ASYMPTOTIC ANALYSIS OF A WEDGE

An asymptotic analysis of large deformation near a corner of a neo-Hookean material has been recently reported.  $^{5,6,13}$  Here we reproduce results relevant to this article. A wedge of angle  $\Phi$  is

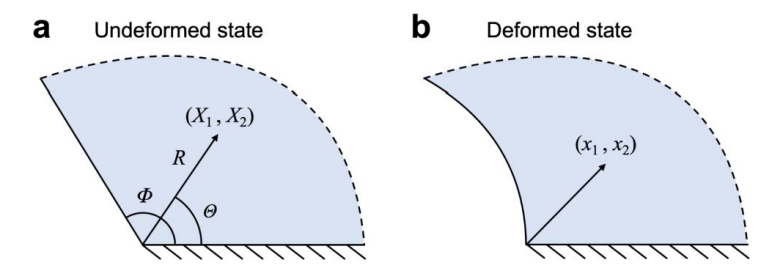


FIG. 3. — A wedge bonded to a rigid substrate undergoing large deformation. (a) Undeformed state. (b) Deformed state.

bonded to a rigid substrate on one edge and is traction free on the other edge. In the undeformed state, a material particle is labeled by polar coordinates  $(R,\Theta)$  and rectangular coordinates  $(X_1,X_2)$  (Figure 3a). The wedge deforms under the plane strain condition. In a deformed state, the same material particle moves to coordinates  $(x_1,x_2)$  (Figure 3b).

The asymptotic analysis assumes that the elastic field near the wedge tip is power-law singular. To leading order, the field of deformation  $x_{\alpha}(R,\Theta)$  is given by

$$x_{\alpha} = c_{\alpha} R^{1 - \frac{m}{2}} \sin\left(\Theta - \frac{\Theta m}{2}\right),\tag{11}$$

where indices labeled with Greek letters can be either 1 or 2,  $c_{\alpha}$  are coefficients, and m relates to the wedge angle  $\Phi$  as

$$m = 2 - \frac{\pi}{\Phi}.\tag{12}$$

Later in this article, we will use the field of energy density  $W(R,\Theta)$ . With Eqs. 1, 11, and  $F_{\alpha\beta} = \partial x_{\alpha}(X_1,X_2)/\partial X_{\beta}$ , the energy density is

$$W = \frac{\mu}{2} (c_1^2 + c_2^2) \left( 1 - \frac{m}{2} \right)^2 R^{-m}. \tag{13}$$

Observe that the asymptotic field of energy density is power-law singular,  $W \sim R^{-m}$ , and has no angular dependence. When the wedge angle is  $\Phi = \pi/2$ , the wedge becomes a 90° corner, m = 0, and the field of energy density is not power-law singular. The deformation and stress fields are also not power-law singular.

When the near-corner field is not power-law singular, Eqs. 12 and 13 are invalid, because neglecting terms in the asymptotic analysis can no longer be justified. Instead, a full-field solution must be obtained to analyze the elastic field near the corner. The elastic field calculated by the finite element method has been previously reported. <sup>5,6</sup> Here, we compute the elastic field with a mesh of a higher resolution and to applied strains of larger magnitude. For other material models, asymptotic analyses of a corner are unavailable. In this article, we use neo-Hookean, Yeoh, and Gent materials in finite element simulations.

## FINITE ELEMENT SIMULATION

We use a commercial finite element software ABAQUS to determine the elastic field. The incompressibility of the material is represented in ABAQUS using hybrid elements and a Poisson's ratio of 0.495. Hybrid elements are provided by ABAQUS. They are used when the material is assumed to be incompressible or nearly incompressible. Since the pressure  $\rho$  is undetermined by the displacement field, hybrid elements introduce an additional degree of freedom to calculate the

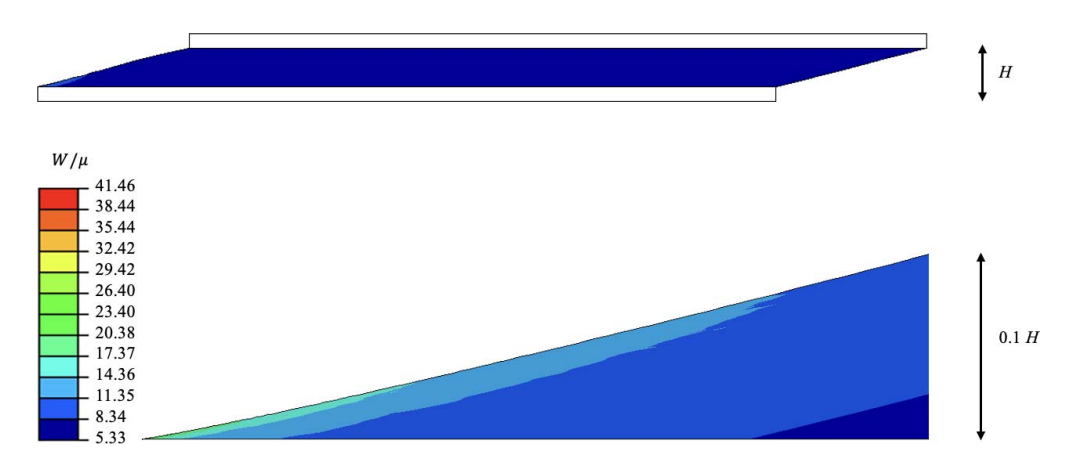


FIG. 4. — Deformation in lap shear at an applied shear strain of  $\gamma = 4$ . Contours of normalized energy density are plotted in the entire sample as well as around a corner. The material is neo-Hookean.

pressure. The displacement field is used to calculate the deviatoric strains and stresses. Using hybrid elements is a standard practice in analyzing hyperelastic materials under plane strain conditions. The substrates are meshed with rigid elements in the simulation. To represent the corner, we use a combination of triangular and quadrilateral elements of quadratic order (CPE8H and CPE6H). We use a refined mesh near the corner, where the mesh becomes 10 times finer for every decade in R. The minimum mesh size near the corner is  $2 \times 10^{-6} H$ . A layout of the mesh can be found in our previous work. The top and bottom surfaces of the stretchable material meet rigid substrates, and the left and right edges of the stretchable material are traction free. ABAQUS provides a rigid element, for which the user can specify either rigid-body displacements or resultant forces, as well as either rigid-body rotation or resultant moment. We use one rigid element to represent the top substrate and another rigid element to present the bottom substrate. The bottom substrate is held fixed by prescribing zero rigid-body displacements and zero rigid-body rotation. The top substrate is prescribed with a horizontal rigid-body displacement d, zero vertical resultant force, and zero rigid-body rotation. We set L/H = 20 and vary d/H from 1 to 32. Thus, for large values of d/H, the condition  $L \gg d$  is not satisfied. A consequence of this situation will be discussed later.

The stretchable material undergoes an inhomogeneous deformation, but the inhomogeneity concentrates near the edges (Figure 4). In the undeformed state, we center a polar coordinate system  $(R,\Theta)$  at the corner. ABAQUS reports a value of energy density for each element. Here, we plot the energy densities of elements in the bottom layer of the soft material for various applied shear strains  $\gamma$  (Figure 5a). For any applied strain, the energy density plateaus near the corner, indicating that the elastic field is bounded. When the applied strain is small, the field at the corner is greatly amplified from the applied field. For applied strains smaller than 1, the elastic field approaches that of the linear elastic singularity. When the applied strain is large, the field at the corner is comparable to the applied field. The energy density has no angular dependence, which is consistent with a bounded elastic field at the corner (Figure 5b). We further confirm that the near-corner field is concentrated and bounded for other material models (Figure 5c,d). We have varied the finite element mesh size to ascertain the convergence of the simulations. Our results show that the magnitude of the energy density near the corner changes negligibly with mesh size once the mesh size around the corner is below  $1 \times 10^{-5} H$ .

Similar to the field of energy density, the field of stress is also bounded and concentrated (Figure 6). The stress components  $\sigma_{11}$  and  $\sigma_{12}$  are much larger than  $\sigma_{22}$  and  $\sigma_{33}$ . This behavior is perhaps unsurprising. Recall that a large portion of the sample is under homogeneous deformation

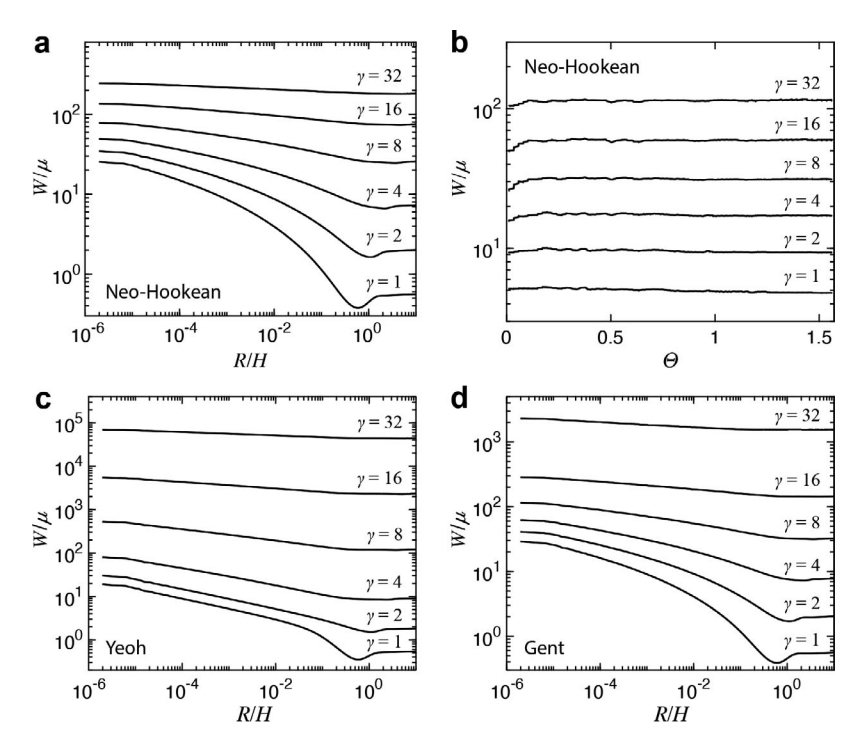


FIG. 5 — Elastic fields are bounded and concentrated near a corner. (a)  $W/\mu$  as a function of R/H at  $\Theta=0$  for the neo-Hookean material and various applied strains. (b)  $W/\mu$  as a function of  $\Theta$  at  $R/H=10^{-3.5}$  for the neo-Hookean material and various applied strains. (c)  $W/\mu$  as a function of R/H at  $\Theta=0$  for the Yeoh material and various applied strains. (d)  $W/\mu$  as a function of R/H at  $\Theta=0$  for the Gent material and various applied strains. The parameters for the Yeoh and Gent materials are the same as those used in Figure 2.

of simple shear (Figure 4). As noted in the "Various Material Models" section, this homogeneous deformation of simple shear generates stresses  $\sigma_{11}-\sigma_{22}=\sigma_{11}-\sigma_{33}=\mu\gamma^2$  and  $\sigma_{12}=\sigma_{21}=\mu\gamma$ . Near the edge of the sample, however, the deformation is inhomogeneous. The near-corner field still has large components of  $\sigma_{11}$  and  $\sigma_{12}$ . This behavior is also found in the simulations using the Yeoh and Gent materials. We note that, by default, ABAQUS reports stress components at the integration points in an element, which we use to plot Figure 6a,b. ABAQUS also provides an option to interpolate stress values at the nodes, which we use to plot Figure 6c,d to reduce scatter in the data.

The near-corner field is bounded but is amplified from the field far from the corner. We define a concentration factor by

$$K = W_{\text{corner}}/W_{\infty}. \tag{14}$$

Here,  $W_{\text{corner}}$  is the energy density at the corner and  $W_{\infty}$  is the energy density far from the corner. Far from the corner, the sample is under homogeneous deformation of simple shear, so that  $W_{\infty} = \mu \gamma^2/2$  for the neo-Hookean material,  $W_{\infty} = \mu \gamma^2/2 + C_2 \gamma^4 + C_3 \gamma^6$  for the Yeoh material, and  $W_{\infty} = -\mu/2J_m \ln(1-\gamma^2/J_m)$  for the Gent material. Since the near-corner field is bounded, K is independent of coordinates R and  $\Theta$ . When  $L \gg H$  and  $L \gg d$ , the boundary value problem has a single length scale, the thickness H. The displacement d is represented by the applied strain,  $\gamma = d/H$ . Thus, the concentration factor K is a function of the applied strain,  $K(\gamma)$ . Our finite element simulations show that this function is insensitive to the material model (Figure 7). In our results,  $W_{\text{corner}}$  is taken at  $R/H = 10^{-4}$  while  $W_{\infty}$  is taken at R/H = 7. When  $\gamma$  is small, the near-corner field approaches the linear

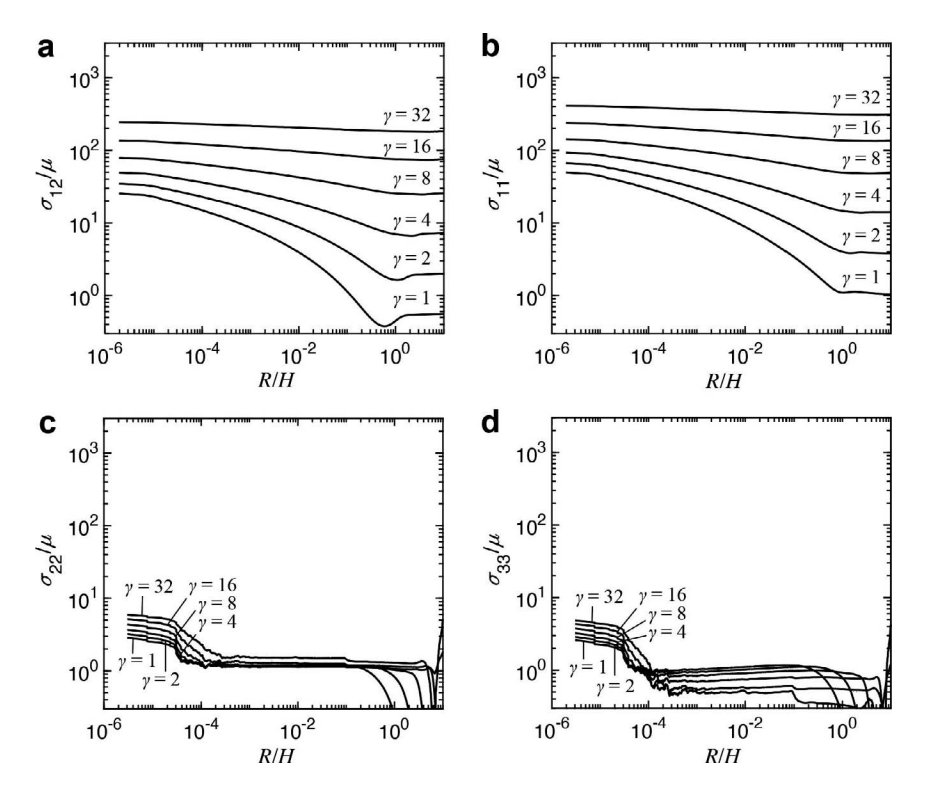


FIG. 6 — The field of true stress near a corner at  $\Theta$ =0, plotted for strains  $\gamma$ =1, 2, 4, 8, 16, and 32. (a)  $\sigma_{12}/\mu$ , (b)  $\sigma_{11}/\mu$ , (c)  $\sigma_{22}/\mu$ , and (d)  $\sigma_{33}/\mu$ . The material is neo-Hookean.

elastic field, which is singular. Consequently,  $K \to \infty$  as  $\gamma \to 0$ . As the applied strain increases, the concentration factor decreases and plateaus.

Incidentally, our calculations assume L/H = 20, which violates the condition  $L \gg d$  for large applied strains. In general, the concentration factor should be a function of both d/H and L/H. We have not studied the effect of L/H.

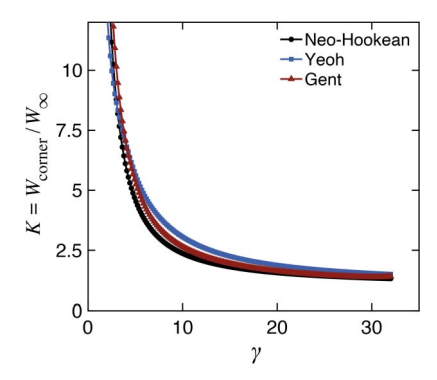


FIG. 7. — Field concentration factor as a function of applied shear strain.  $W_{\rm corner}$  is taken at  $R/H = 10^{-4}$  and  $\Theta = 0$ .  $W_{\infty}$  is taken at R/H = 7 and  $\Theta = 0$ .

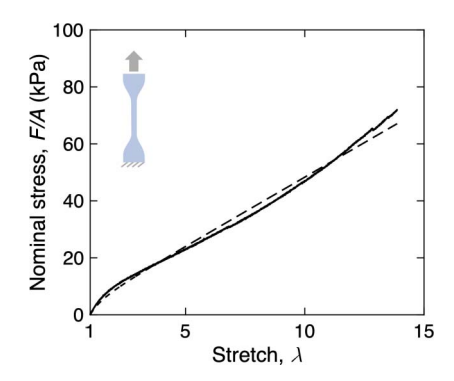


FIG. 8. — Uniaxial tension of a highly stretchable PAAm hydrogel (N = 1000). The dashed line represents an incompressible neo-Hookean material with shear modulus  $\mu = 4.84$  kPa.

## LAP SHEAR OF A HIGHLY STRETCHABLE POLYACRYLAMIDE HYDROGEL

We prepare polyacrylamide (PAAm) hydrogels by free radical polymerization of acrylamide monomer (A8887, Sigma Aldrich, St. Louis, MO, USA), using N,N'-methylenebisacrylamide crosslinker (M7279, Sigma Aldrich) and 2-hydroxy-4'(2-hydroxyethoxy)-2-methylpropiophenone photoinitiator (410896, Sigma Aldrich). The molar ratios of water, crosslinker, and initiator to monomer are  $25, 5 \times 10^{-3}$ , and  $5 \times 10^{-4}$ , respectively. The resulting hydrogels are 86 wt% water. The number of monomers between two crosslinks for these hydrogels is estimated as  $N \sim 1/2C$ , where C is the molar ratio of crosslinker to monomer. <sup>14</sup> The resulting hydrogels have N=1000. The stress–stretch curve for the as-prepared hydrogel is measured in uniaxial tension (Figure 8). The stress–stretch curve is fit well by the neo-Hookean model.

We next cut rectangular samples from a large sheet of hydrogel with a razor blade. A sample of thickness H, length L, and width B is then glued between two polyester substrates (8567K92, McMaster-Carr, Elmhurst, IL, USA) using cyanoacrylate (Krazy Glue). The edges of the hydrogel meet the surfaces of the substrates to form  $90^{\circ}$  corners. The substrates are prepared with lengths longer than L, and the unbonded sections of the substrates are clamped in grips of a tensile tester (5966, Instron, Norwood, MA, USA). In the lap shear test, the tensile tester pulls the substrates relative to each other by a distance d and measures the force F. The grips of the tensile tester are positioned such that the two substrates are parallel prior to testing. During the test, the clamps do not constrain the bending of the substrates near the gel, do not constrain the thickness of the gel, and do not prevent rotation of the gel. The intention of a lap shear test is to subject the hydrogel to homogeneous shear strain  $\gamma = d/H$  and homogeneous shear stress

$$\tau = F/BL. \tag{15}$$

To maintain a plane strain deformation, we have fabricated the samples such that  $B \gg H$ .

The above homogeneous deformation does not apply to the hydrogel near the corners. To ensure the homogeneous deformation prevails in a large portion of the hydrogel away from the corners, we consider the following conditions. First, when the length of the hydrogel is extremely long, the substrates can no longer be modeled as rigid materials. The elasticity of the substrates will transmit shear in the hydrogel to tension in the substrates. This behavior, called shear lag, identifies a length scale <sup>15–17</sup>:

$$L_0 = \sqrt{\frac{E_s H_s H}{\mu}},\tag{16}$$

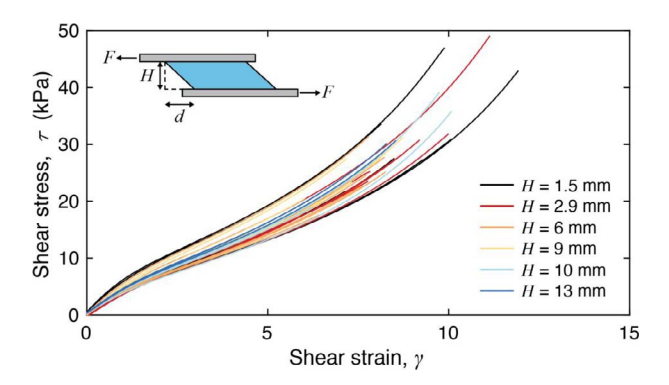


FIG. 9. — Lap shear of a highly stretchable PAAm hydrogel (N = 1000). Shear stress–strain curves of samples of various thicknesses.

where  $E_s$  and  $H_s$  are Young's modulus and the thickness of the substrate, respectively, and  $\mu$  and H are the shear modulus and thickness of the hydrogel, respectively. Taking H=1 mm,  $\mu=4.5$  kPa,  $H_s=0.25$  mm, and  $E_s=3$  GPa, we estimate  $L_0\sim 40$  cm. We prepare samples such that  $H\ll L\ll L_0$ . Second, when the relative displacement between the two substrates is too large, such that d is comparable to or even larger than L, the flexibility of the substrates will cause the hydrogel to rotate. These two considerations suggest that homogeneous shear deformation prevails in a large portion of the hydrogel under the conditions  $H\ll L\ll L_0$  and  $d\ll L$ . When the dimensions are within this range, lap shear generates a simple shear deformation in a large portion of the hydrogel away from the corners.

We have used thin polyester sheets as substrates based on the following considerations. First, thin substrates are flexible. While bent, the substrate meets the surface of the gel at a line, such that the substrate can be glued to the gel without trapping bubbles along the interface. Bubbles could concentrate stress and should be avoided. Second, thin sheets are easily processed from bulk material. Third, when  $L_0 \gg L$ , flexible and inflexible substrates deform the gel similarly and produce similar conditions at rupture. <sup>17</sup>

We measure the shear stress-strain curves for samples of the polyacrylamide hydrogel of various thicknesses (Figure 9). For each thickness, several samples are tested. For each sample, a shear stress-strain curve is recorded up to fracture. These shear stress-strain curves are nonlinear, indicating that the PAAm hydrogel deviates from the neo-Hookean material somewhat.

The shear stress–strain curves differ from sample to sample. To see this difference clearly, we characterize the shear stress–strain curve of each sample with four properties. The slope of the curve at small strains defines the shear modulus  $\mu$ . The point of fracture defines the critical strain  $\gamma_c$  and critical stress  $\tau_c$ . The area under the curve defines the energy density at fracture  $W_c$ .

For samples of any given thickness, each of the four properties has a comparable scatter from sample to sample (Figure 10). For samples of different thicknesses, all four properties do not vary much with thickness. Also included are data of a less stretchable PAAm hydrogel (N=100), which were obtained in our previous work.<sup>6</sup> Whereas  $W_c$  of the highly stretchable gel (N=100) is independent of thickness,  $W_c$  scales with thickness as  $W_c \sim H^{-0.8}$  when the gel has limited stretchability (N=100). We have previously explained this dependence for the brittle gel by analyzing the linear elastic field near the corner.

Our experimental results demonstrate that, at fracture, the critical applied strain, stress, and energy density are independent of the thickness of the material. We interpret this experimental finding as follows. First, as shown in our finite element simulations, for highly stretchable materials, the elastic field near the corner is bounded. Second, the energy density at the corner depends on the

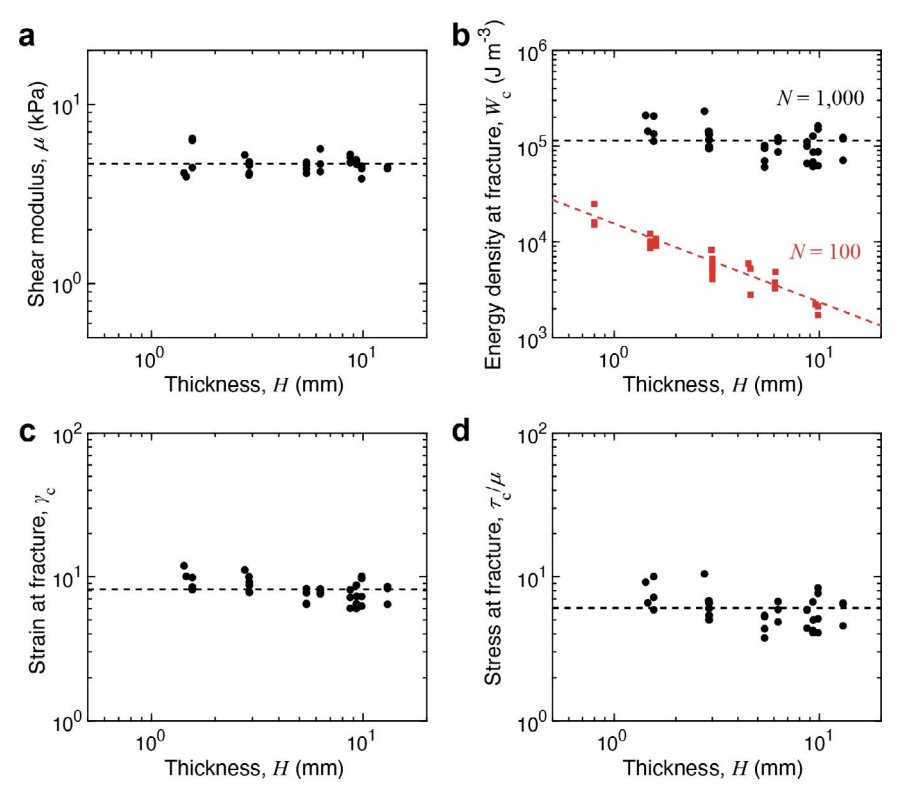


FIG. 10. — Mechanical properties of samples of a highly stretchable PAAm hydrogel (N=1000) with various thicknesses. (a) Shear modulus  $\mu$ . (b) Energy density at fracture  $W_c$ . (c) Shear strain at fracture  $\gamma_c$ . (d) Shear stress at fracture  $\tau_c$ . The dashed lines indicate the mean values. The data of  $W_c$  for the PAAm hydrogel of N=100 are replotted with permission from ref 6, where the dashed line indicates the scaling  $W_c \sim H^{-0.8}$ .

applied energy density according to  $W_{\text{corner}} = KW_{\infty}$ , where K is a function of the applied strain  $\gamma$ . At a fixed applied strain, the field around the corner is fixed in both its amplitude and type of deformation. Third, fracture initiates from a corner when the energy density at the corner  $W_{\text{corner}}$  reaches a critical value, called the work of fracture,  $W_f$ . The work of fracture is assumed to be a material property independent of thickness. <sup>18</sup> The above considerations are consistent with the experimental observation that the critical applied strain is independent of the thickness. Thus, the critical applied shear stress and critical applied energy density should also be independent of thickness. Consequently, our assumption that  $W_f$  is a material property is consistent with the experimental observation that the critical applied energy density is independent of the thickness.

The above discussion assumes that  $L\gg H$  and  $L\gg d$ , so that the elastic field depends on lengths through a single dimensionless ratio, the applied shear strain  $\gamma=d/H$ . In our experiment, these conditions are not always satisfied. For example, when the sample is thick and the applied strain is large, using a very long sample has been experimentally inconvenient. Under such a condition, because L is not long enough, the sample rotates somewhat when the substrates are pulled. The field around the corner will vary with two dimensionless parameters, d/H and L/H. In particular, at a fixed applied strain  $\gamma=d/H$ , both the amplitude and type of deformation near the corner will vary with L/H. This effect may alter the results for samples of large thicknesses tested here.

In general, for a given material, the work of fracture  $W_f$  varies with type of deformation. For instance, the work of fracture under shear differs from that under uniaxial tension. Consequently, the critical applied shear strain should vary with L/H, since varying L/H can alter the type of deformation. In our experiment, we have not varied L/H systematically over a large range. Our experiments do not show significant deviation from a constant critical applied strain.

## CONCLUDING REMARKS

In summary, we have shown that the elastic field near a corner of a highly stretchable material is concentrated but bounded. The theory of elasticity has no length scale. Under the condition that lap shear is characterized by a single length, the thickness of the stretchable material, the elastic field is independent of any length once the spatial coordinates are normalized by the thickness. We lap shear samples of a highly stretchable hydrogel of various thicknesses. For all samples, fracture initiates from the corners, at a critical load independent of thickness. These experimental findings agree with the computational prediction that the large-deformation elastic field near the corner is concentrated but bounded. Our findings have implications beyond lap shear. For example, the findings also apply to a composite in which a crack in a stretchable material impinges on a rigid material.

## **ACKNOWLEDGEMENTS**

This work was supported by MRSEC (DMR-2011754) and by the Air Force Office of Scientific Research (FA9550-20-1-0397). J.S. was supported by the NSF Graduate Fellowship (DGE1745303).

## REFERENCES

```
<sup>1</sup>M. L. Williams, J. Appl. Mech. 19, 526 (1952).
```

<sup>&</sup>lt;sup>2</sup>F. Erdogan and V. L. Hein, *Int. J. Fract. Mech.* **7**, 317 (1971).

<sup>&</sup>lt;sup>3</sup>E.D. Reedy and T. R. Guess, J. Adhes. Sci. Technol. 9, 237 (1995).

<sup>&</sup>lt;sup>4</sup>M. L. Dunn, W. Suwito, and S. Cunningham, Int. J. Solids Struct. 34, 3873 (1997).

<sup>&</sup>lt;sup>5</sup>C. Y. Hui, B. Zhu, and M. Ciccotti, *Int. J. Fract.* **238**, 71 (2022).

<sup>&</sup>lt;sup>6</sup>J. Steck, S. Hassan, and Z. Suo, *J. Mech. Phys. Solids* **170**, 105115 (2023).

<sup>&</sup>lt;sup>7</sup>A. N. Gent, J. B. Suh, and S. G. Kelly, *Int. J. Nonlinear Mech.* **42**, 241 (2007).

<sup>&</sup>lt;sup>8</sup>R. Long, C. Y. Hui, J. P. Gong, and E. Bouchbinder, *Annu. Rev. Condens. Matter Phys.* 12, 71 (2021).

<sup>&</sup>lt;sup>9</sup>C. O. Horgan and J. G. Murphy, *Soft Matter* **13**, 4916 (2017).

<sup>&</sup>lt;sup>10</sup>M. J. Mooney, J. Appl. Phys. 11, 582 (1940).

<sup>&</sup>lt;sup>11</sup>O. H. Yeoh, RUBBER CHEM. TECHNOL. **66**, 754 (1993).

<sup>&</sup>lt;sup>12</sup>A. Gent, RUBBER CHEM. TECHNOL. **69**, 59 (1996).

<sup>&</sup>lt;sup>13</sup>C. Mo, J. R. Raney, and J. L. Bassani, J. Mech. Phys. Solids 158, 104653 (2022).

<sup>&</sup>lt;sup>14</sup>J. Kim, G. Zhang, M. Shi, and Z. Suo, *Science* **374**, 212 (2021).

<sup>&</sup>lt;sup>15</sup>H. L. Cox, Br. J. Appl. Phys. 3, 72 (1952).

<sup>&</sup>lt;sup>16</sup>C. Y Hui, Z. Liu, H. Minsky, C. Creton, and M. Ciccotti, *Soft Matter* **14**, 9681 (2018).

<sup>&</sup>lt;sup>17</sup>Y. Wang, X. Yang, G. Nian, and Z. Suo, *J. Mech. Phys. Solids.* **143**, 103988 (2020).

<sup>&</sup>lt;sup>18</sup>C. Chen. C. Wang, and Z. Suo, *Extreme Mech. Lett.* **10**, 50 (2017).